

## Hadronic Final State in Deep-inelastic Scattering at HERA<sup>a</sup>

Tancredi Carli

*Max-Planck-Institut für Physik, Werner-Heisenberg-Institut, Föhringer Ring 6,  
D-80805 München, Germany, e-mail: h01rtc@rec06.desy.de*

*On behalf of the H1 and ZEUS collaborations.*

Data on the hadronic final state of deep-inelastic events at the  $e^\pm p$  collider HERA are reviewed. Fragmentation properties in the current region extracted from charged particle spectra are compared to  $e^+e^-$  and fixed target experiments at lower center of mass energies. A measurement of the strong coupling constant from integrated jet rates is presented and prospects to extract the gluon density in the proton by tagging vector mesons are discussed. Data on the inclusive mean transverse energy together with the transverse momentum distribution of single charged particles indicate an increased gluon activity in the central rapidity region when the phase space is enlarged. The measurement of the forward jet cross-section is discussed. Keeping the phase space fixed, the mean transverse energy and the mean charged multiplicity for certain rapidity ranges is found to behave analogously to  $p\bar{p}$  collisions.

### Introduction

The large center of mass energy ( $\sqrt{s} \approx 300$  GeV) available at the  $e^\pm p$  collider HERA offers a large phase space for production of hadrons in deep-inelastic scattering (DIS). This allows the detailed characteristics of the hadronic final state to be probed in a previously unexplored kinematic domain.

In the quark parton model (QPM) the photon scatters elastically on a quark freely moving in the proton. This is a good approximation when small distances are probed at large momentum transfers  $Q^2$ . The kinematics of the scattering process is described by the longitudinal momentum fraction of the quark with respect to the proton momentum ( $x$ ) and by the resolution of the photon probing the proton structure ( $Q^2$ ). These variables are defined in a general way in Fig.1 as Lorentz invariants. At HERA,  $x$  values down to a few  $10^{-5}$  can be reached and  $Q^2$  ranges from low values where the photon is quasi on-shell to very large ones resolving - with the present statistics - distances<sup>1</sup> down to  $\approx 10^{-16}$  cm.

Perturbative QCD plays a key rôle in the understanding of the complex mechanism governing the multi-particle final state. For very short times (corresponding to short distances) before and after the hard interaction of a virtual photon with a parton in the proton, the partons are far away from their mass shell and can be treated as quasi free particles. This first primary scatter-

---

<sup>a</sup>Invited talk given at XVI Int. Conf. on Physics in Collision, Mexico City, June 1996.

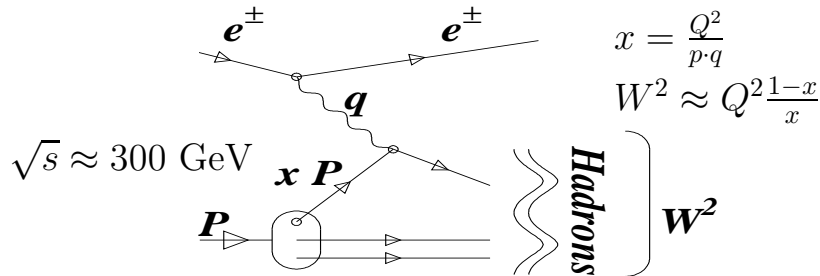


Figure 1: Diagram of a simple electron-proton scattering at HERA.

ing process can be perturbatively described by QCD. Then long range forces become more and more important and quarks with very low virtualities form bound states leading to the observable hadrons.

The multi-purpose HERA detectors allow, in addition to the scattered electron, a large part of the hadronic final state to be measured. Provided that the transition from partons to hadrons can be properly modeled, this opens the possibility to study the underlying parton dynamics using exclusive observables built on particle spectra, jets or energy depositions. Variables based on the hadronic final state can be defined for specific rapidity ranges such that e.g. properties of hadrons close to the proton remnant can be investigated. It is also possible to isolate the current region where the hard subprocess induced by the photon virtuality has taken place and to compare with results obtained in  $e^+e^-$  annihilation. An advantage of HERA is that most measurements can be performed at a variable scale. The mean multiplicity of charged particles can e.g. be studied as function of  $W$  and the strong coupling constant  $\alpha_s$  can be extracted from integrated jet rates in different bins of  $Q^2$ . The phenomenon of diffraction in DIS is covered by M. Derrick in these proceedings.

### Particle spectra in the current region

A natural reference frame to study properties of the hadronic final state is the hadronic center of mass system (cms) where the virtual photon and the proton have momenta of equal magnitude and point in opposite directions. Within the QPM, the photon and the incoming quark collide in this frame head-on and no transverse momentum ( $P_T^*$ ) is transferred to the struck quark. The  $P_T^*$  of the measured hadrons is only produced during the fragmentation of the quark and therefore maximally limited to the typical inverse size of a hadron. Higher values of  $P_T^*$  can only originate from gluon emissions before and after the hard

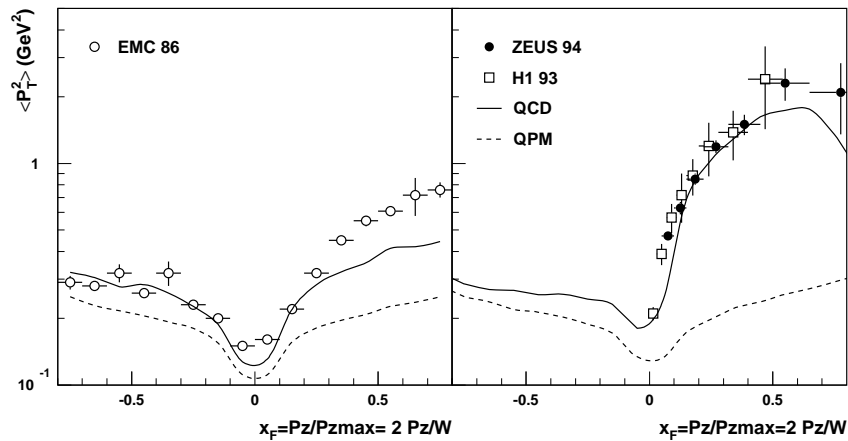


Figure 2: Mean squared transverse momentum as function of the scaled longitudinal momentum for charged particles in the cms. HERA data are indicated by the open squares (H1) and the closed circles (ZEUS). The data from a  $\mu^\pm p$  fixed target experiment at  $\sqrt{s} = 23$  GeV (EMC) are given as open circles. The prediction from ARIADNE as a QCD model (solid) and the naive quark parton model (dashed) are superimposed as lines.

interaction. Neglecting gluon radiation the longitudinal momentum ( $P_z^*$ ) of the struck quark is given by  $W/2$ . Correspondingly the target remnant moves in opposite direction with  $-W/2$ . A natural variable to study the longitudinal momenta of the emerging hadrons is therefore  $x_F = P_z^*/P_{z\max}^* = 2P_z^*/W$ .

The importance of processes involving QCD radiation is illustrated in Fig. 2 where the  $\langle P_T^{*2} \rangle$  versus the  $x_F$  of charged particles is shown. Without allowing for parton radiation the  $\langle P_T^{*2} \rangle$  is limited to  $0.3 \text{ GeV}^2$  (dotted line). Much larger  $\langle P_T^{*2} \rangle$  are found in the HERA data<sup>2,3</sup> and they are well described by a QCD model (solid line). In the target hemisphere ( $x_F < 0$ ), where no HERA measurements are available yet, the  $\langle P_T^{*2} \rangle$  is less prominent and only little  $P_T^*$  is produced by gluon radiation. This can be understood in terms of the extended colour charge distribution suppressing small wavelength gluon radiation. At lower center of mass energies where less phase space for gluon radiation is available, the  $\langle P_T^{*2} \rangle$  is even more limited. This can be seen e.g. in the data of the EMC collaboration<sup>4</sup>, a  $\mu^\pm p$  fixed target experiment at  $\sqrt{s} = 23$  GeV. In this kinematic region QCD models do not significantly add transverse momenta to the naive expectation from the QPM and have moreover difficulties to describe the data<sup>5</sup>.

Detailed comparisons between  $e^+e^-$  and  $e^\pm p$  collisions are most suitably carried out in the Breit frame. In this frame the only non-zero space-like

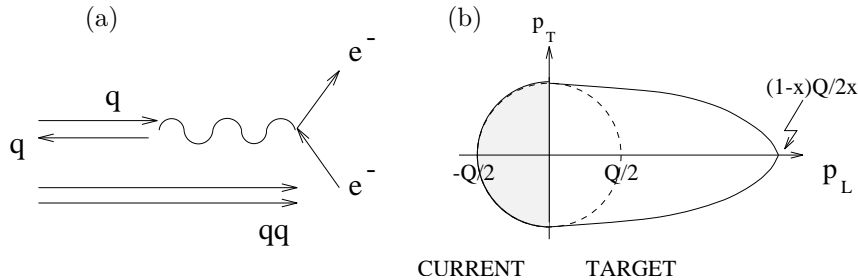


Figure 3: (a) Sketch of a simple photon-quark collision in the Breit frame (b) Phase space for the longitudinal and transverse momenta of single particles in this frame.

component of the photon four-momentum is given by  $P'_z = -2xE_P$  with  $E_P$  the proton beam energy. Within the QPM, the struck quark enters with  $P'_z = Q/2$  and collides on the virtual photon as on a 'brick wall', from which it simply rebounds with  $P'_z = -Q/2$  (see Fig. 3a). The particles scattered in the hemisphere of the struck quark ( $P'_z < 0$ ) behave like those produced in one hemisphere of an  $e^+e^-$  annihilation event at  $s = Q^2$ . As in  $e^+e^-$  in this hemisphere properties of longitudinal particle momenta should only depend on  $Q$ . The opposite hemisphere ( $P'_z > 0$ ) contains the proton remnant and moves with  $P'_z = (1-x)E_P = (1-x)Q/2x$  (see Fig. 3b).

The linear rise of (twice) the mean charged particle multiplicity ( $\langle n \rangle$ ) with  $\log Q$  for DIS measured at HERA<sup>6,7</sup> is shown in Fig. 4a. For  $Q > 7$  GeV, DIS and  $e^+e^-$  data<sup>8</sup> reasonably agree. However, when going to lower  $Q$  the differences between  $e^+e^-$  and  $e^\pm p$  collisions become more and more distinct. A higher multiplicity is observed in  $e^+e^-$  data taken by MARK1. A clear dependence of  $\langle n \rangle$  on  $x$  is observed when comparing the HERA data at low  $x$  with the  $\nu p$  data of a fixed target experiment at FNAL<sup>9</sup> at  $x$  close to 0.1. While agreeing at high  $x$  with the  $e^+e^-$  data, in DIS the current hemisphere is more and more depopulated at low  $x$  where higher order parton emission become increasingly important. This is due to an asymmetric migration from the current to the target hemisphere, not present in  $e^+e^-$  annihilation.

The distribution of the scaled longitudinal momenta  $x_p = P'_z/P'_{z\max} = 2P'_z/Q$  of single charged particles allows fragmentation to be studied in further detail. The fragmentation function  $1/\sigma_{\text{tot}} d\sigma/dx_p$ , with  $1/\sigma_{\text{tot}}$  the total cross-section in a particular  $(x, Q^2)$  bin, characterizes the complete process of hadron formation including QCD parton evolution and the non-perturbative transition from partons to hadrons. It is not calculable in perturbative QCD, but can, as the structure function  $F_2$ , be evolved in  $Q^2$  given a measured starting distribution.  $1/\sigma_{\text{tot}} d\sigma/dx_p$  rises with decreasing  $x_p$  and turns over at low

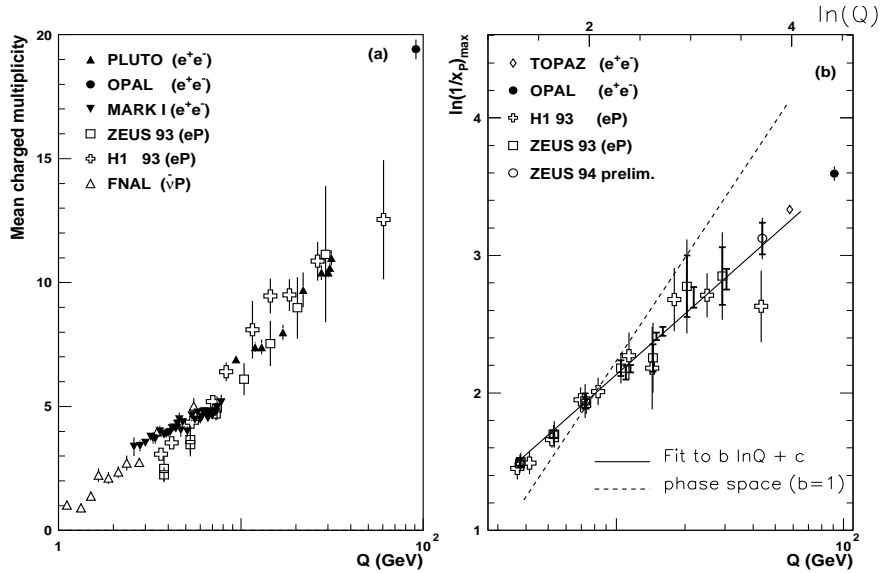


Figure 4: Mean multiplicity of charged particles (a) and the peak position of the  $\ln 1/x_p$  distribution (b) as function of  $Q$  in  $e^+e^-$ ,  $e^\pm p$  and  $\bar{\nu}p$  collisions. The  $e^\pm p$  data are measured in the Breit frame and the multiplicity is multiplied by a factor of two.

$x_p$ . This region can be expanded by transforming  $x_p$  to  $\ln 1/x_p$  (see Fig.5a and b). At small  $x_p$ ,  $1/\sigma_{\text{tot}} d\sigma/dx_p$  is affected by coherence of soft gluons while at large  $x_p$  it can be used to determine  $\alpha_s$ .

At small  $x_p$  the phase space for soft gluon emission is reduced to an angular ordered region caused by destructive interference. This suppression of soft gluons is predicted by QCD, since the power of gluons to resolve individual colour charges should be diluted with increasing wavelength<sup>10</sup>. Assuming that the basic features of a distribution for partons are preserved for the measured hadrons, this results then in a slower rise of the particle multiplicity and of the peak position of the  $\ln 1/x_p$  distribution with  $\log Q$  than simply expected from the increased longitudinal phase space. Fig. 4b shows the evolution of the  $\ln 1/x_p$  peak position measured for particles having  $x_p > 0$ . The same linear rise with  $\log Q$  is observed in  $e^+e^-$  data<sup>11</sup> which provides a hint of a universal behaviour of quark fragmentation. As the data become more precise, expected differences between  $e^+e^-$  and DIS fragmentation should become manifest due to e.g. different quark flavour composition. The modified leading logarithm approximation (MLLA) of QCD is able to describe this evolution down to very low  $Q$  (solid line). The coherent evolution is clearly favoured by the data. It can, however, not be excluded that a similar attenuation of the slope could

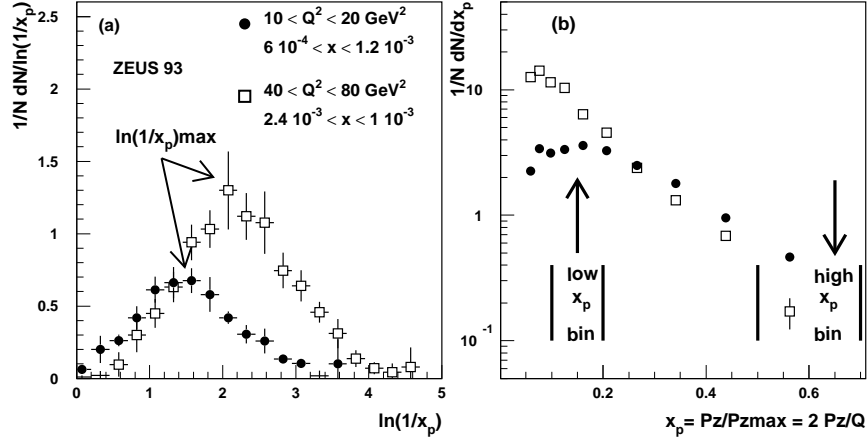


Figure 5: Distribution of the scaled longitudinal momentum  $x_p = 2P'_z/Q$  for charged particles in the Breit frame in two  $(x, Q^2)$  bins measured by ZEUS (b). The same data after transforming  $x_p$  to  $\ln 1/x_p$  (a).

also be caused by effects during the hadronisation phase<sup>12</sup>.

The evolution of  $1/\sigma_{\text{tot}} d\sigma/dx_p$  in different bins of  $x_p$  with  $Q^2$  is shown in Fig. 6<sup>16</sup>. With increasing  $Q^2$ ,  $1/\sigma_{\text{tot}} d\sigma/dx_p$  increases at low  $x_p$  and decreases at high  $x_p$ . When more phase space is available more gluons can be emitted which results in a softening of the particle spectra. Therefore more particles at low  $x_p$  and less at large  $x_p$  are observed. These scaling violations can be treated in an analogous way as in the proton structure function analysis<sup>13</sup> to extract the strong coupling constant  $\alpha_s$ . Such a measurement has been performed<sup>14</sup> using LEP data together with lower energy  $e^+e^-$  data. At HERA this method could be applied in one single experiment. However, to avoid the region where migrations between the current and target hemisphere become important, one has to restrict the analysis to  $Q^2 > 100 \text{ GeV}^2$ . Scaling violations are observed, but more data is needed to get the necessary precision at large  $x$  and  $Q^2$  for a competitive extraction of  $\alpha_s$ . Since the scaling violation in the fragmentation function are only of logarithmic nature, the achievable error on  $\alpha_s$  will, even with high statistics, not be competitive with the present error on the world average<sup>17</sup>.

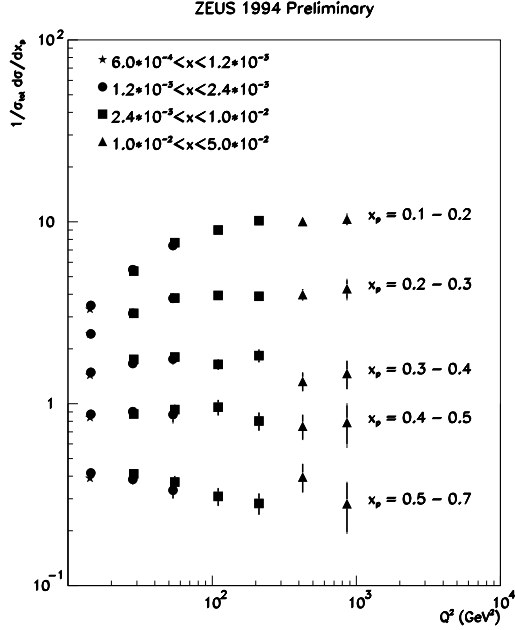


Figure 6:  
 $1/\sigma_{\text{tot}} d\sigma/dx_p$  in the Breit frame for different bins of the scaled longitudinal momentum  $x_p$  as function of  $Q^2$ . The data have been measured by ZEUS.

### Determination of the strong coupling constant using jets

The high values of  $W$  reachable at HERA allow clean jets to be observed in the hadronic final state. Events with two jets in addition to the one close to the beam carrying the remnants of the proton (2+1 jet events) are produced in leading order of  $\alpha_s$  by processes either induced by a gluon in the proton (Fig. 7a) or by a quark radiating a gluon before or after interacting with the photon (Fig. 7b). The cross-section of both processes is proportional to  $\alpha_s$ . For the gluon initiated processes in addition precise knowledge of the gluon density in the proton  $g(x, Q^2)$  is required to calculate the cross-section. The sensitivity to both  $\alpha_s$  and  $g(x, Q^2)$  can be used to simultaneously extract these quantities. Such an analysis is however theoretically and experimentally difficult. The analysis is therefore split in two kinematic regions. At low  $x$  and  $Q^2$  the gluon initiated processes dominate. This can be used to extract  $g(x, Q^2)$  by assuming a value of  $\alpha_s$  and statistically subtracting the quark induced processes. At large  $x$  and  $Q^2$  the parton densities are well known and the proportionality coefficients between the 2+1 jet rate and  $\alpha_s$  are given by next-to-leading order QCD calculations<sup>18</sup>. The measurement of the ratio of 2+1 jet events to all events at some value of  $Q$  allows therefore  $\alpha_s(Q)$  to be extracted. By evaluating  $\alpha_s(Q)$  in different  $Q$  bins the running of the strong coupling constant can be tested in one experiment.

For the  $\alpha_s$  measurement only the kinematic range of high  $Q$  is considered

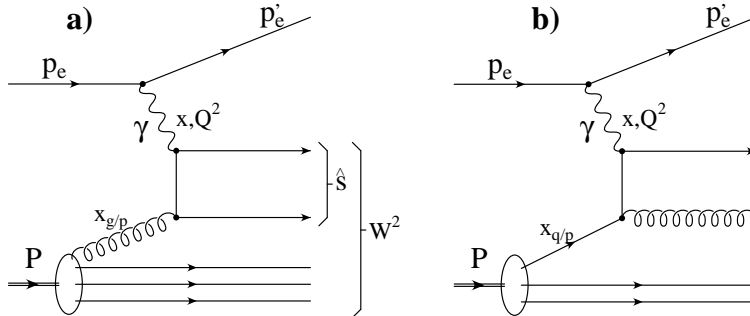


Figure 7: Feynman diagrams for the production of 2 + 1 jet events to first order of  $\alpha_s$  in  $e^\pm p$ -collisions.

to reduce the uncertainties from hadronisation. To avoid the region where higher order gluon emission become important, only events at high  $x$  are considered, and also, the experimentally difficult, very forward region is excluded. Jets are experimentally and theoretically defined by the JADE clustering algorithm<sup>19</sup>. Three values of  $\alpha_s(Q)$  extracted by the H1<sup>20</sup> and ZEUS<sup>21</sup> collaboration are shown in Fig. 8. For increasing values of  $Q$ ,  $\alpha_s(Q)$  decreases as predicted by the renormalisation group equation shown for  $\Lambda_{\overline{\text{MS}}}$  between 100 and 300 MeV (solid lines). An extrapolation to  $\alpha_s(M_z)$  yields:

$$\text{H1 93 : } \quad \alpha_s(M_z) = 0.123 \pm 0.012(\text{stat}) \pm 0.013(\text{syst.})$$

$$\text{ZEUS 94 : } \quad \alpha_s(M_z) = 0.117 \pm 0.005(\text{stat}) + 0.005(\text{exp.}) \pm 0.007(\text{th.})$$

which is consistent with other values obtained from a large variety of different processes as shown Fig. 8 (see<sup>22</sup> for references). The agreement found in  $e^+e^-$ ,  $e^\pm p$  and  $p\bar{p}$  collision for reactions at very different scales is an important and successful test of QCD. The error on the HERA measurement are even with the present limited statistics already competitive.

The dominant experimental errors stem from the uncertainty on the energy scale for hadrons, the model dependence of assigning the jets to partons and the phenomenological description of the hadronisation process. Furthermore the renormalisation scale and the choice of the input parton density systematically influences the result. For consistency it would be necessary to simultaneously fit  $\alpha_s$  used in the parton densities, but this effect is negligible in the phase space region where the HERA analysis has been performed<sup>23</sup>. Recently a new next-to-leading order calculation<sup>24</sup> became available allowing to analyze the data using all available jet definition schemes and to impose any acceptance cut on the final state particles. Moreover different renormalisation and factorisation

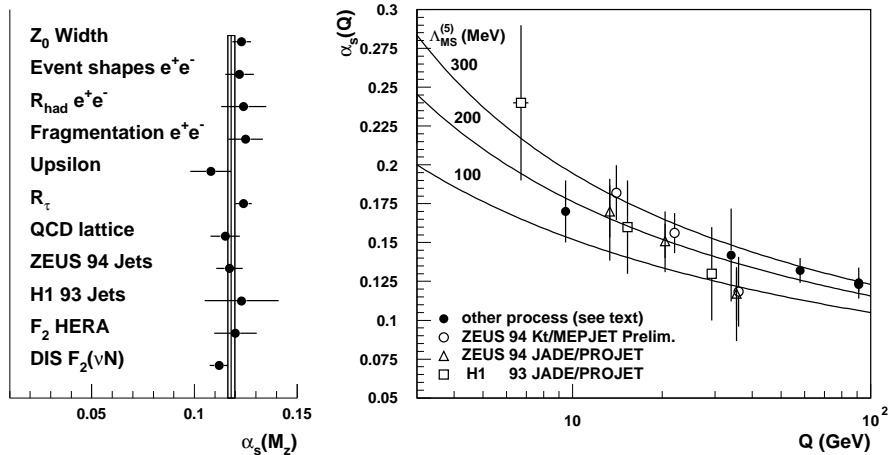


Figure 8: Left: Values and total error of  $\alpha_s(M_Z)$  from various processes. The solid line indicates the world average and the band its total error. Right:  $\alpha_s(Q)$  from HERA (open symbols) and other processes with increasing  $Q$  (closed circles):  $\Gamma_\Upsilon$  and  $\sigma_{\text{had}}/\sigma_{\text{tot}}$ , event shapes and  $\Gamma_{\text{hadron}}/\Gamma_{\text{epton}}$  in  $e^+e^-$ . The predictions of the renormalisation group equation for three values of  $\Lambda_{\overline{\text{MS}}}^{(5)}$  are superimposed as lines.

scales (e.g.  $P_T^*$  instead of  $Q$ ) can be tested. These calculations will allow the theoretical systematic errors to be better assessed. One of the insights gained from these studies is that the cone<sup>25</sup> or  $k_T$ <sup>26</sup> jet algorithm seem to be better suited for precision QCD tests than the JADE scheme, since the variation of the cross section when going from leading to next-to-leading order is much smaller<sup>27</sup>. Moreover, these jet algorithms are less dependent on the choice of the hard scale and allow a larger phase space to be covered. The ZEUS collaboration has reanalyzed their data<sup>28</sup> using the  $k_T$  algorithm. The preliminary values of  $\alpha_s(Q)$  obtained in three bins of  $Q$  are shown<sup>b</sup> in Fig. 8. They are consistent with the results obtained with the JADE algorithm.

### On the determination of the gluon density in the proton

The dynamics of the strong interaction at high momentum scales, corresponding to short distances, is successfully described by perturbative QCD. A vital ingredient of any QCD prediction for a reaction where a nucleon is involved is an assumption about the parton distribution in the nucleon needed to calculate an observable in terms of basic QCD subprocesses at the partonic level. This parton density function  $f(x, Q^2)$  is the probability to find a parton within a

<sup>b</sup>Only the statistical errors are included in the figure.

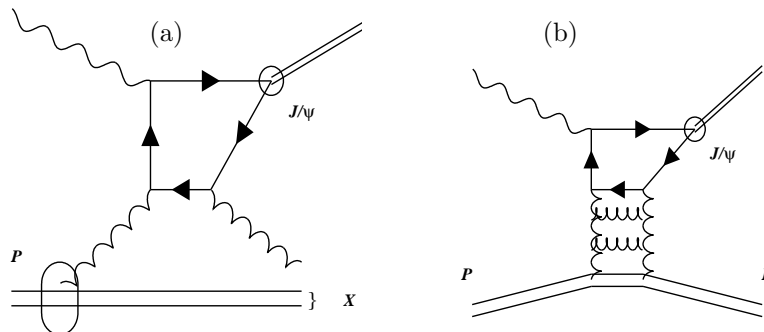


Figure 9: *Leading Feynman diagram for inelastic  $J/\psi$  production (a) and a QCD inspired model for elastic  $J/\psi$  production (b) in  $\gamma p$ -collisions.*

nucleon carrying a fraction  $x$  of its momentum when probed by a particle with virtuality  $Q^2$ . Once  $f(x, Q^2)$  has been determined in one reaction it can be used for any other prediction.

In deep-inelastic scattering the collinear singularities encountered when calculating the hard subprocess to order  $\alpha_s$  are absorbed in the parton densities. The parton densities are usually evolved by the DGLAP equations<sup>29</sup>, presently known in leading and next-to-leading order, which describe the splitting of a parton. Once the parton densities have been measured at some  $Q^2$  value they can be evolved to any point in the kinematic plane. The parametrisation of the input distribution is obtained by a global fit to a large variety of data. Two different strategies have been adopted. Martin, Roberts and Stirling<sup>30</sup> and the CTEQ collaboration<sup>31</sup> parametrise the starting distribution at some  $Q_0^2$  ( $1 - 5 \text{ GeV}^2$ ) and fit then the parameters to data by evolving  $f(x, Q_0^2)$ . A dynamical approach is pursued by Glück, Reya and Vogt<sup>32</sup> where only valence like parton densities with  $f(x=0, Q_0^2) = 0$  are assumed at a very low input scale  $Q_0^2 = 0.34 \text{ GeV}^2$ . The gluon and the sea quark distributions are then generated radiatively. This procedure predicted the steep rise of the structure function <sup>c</sup>  $F_2$  with decreasing  $x$  and moreover the slowing down of this rise towards lower  $Q^2$ .

The parton distributions are well constrained for large  $x$  where a lot of data are available. However, in the small  $x$  regime where gluons play a crucial rôle, they are not well known. HERA has therefore the unique possibility to investigate the distribution of the gluon density in the proton. The scaling violation

<sup>c</sup>see p.14-15 for more details and references.

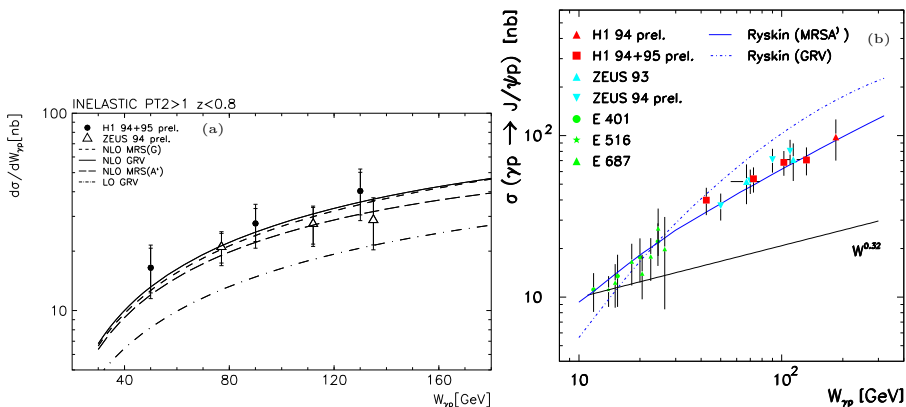


Figure 10: Cross-section for inelastic (a) and elastic (b)  $J/\psi$  production as function of  $W_{\gamma p}$  for HERA and fixed target photoproduction data. Predictions of the Ryskin model for different parameterisations of the gluon density are superimposed. The solid line below the data indicates a simple parametrisation  $\sigma_{\gamma p} \sim W_{\gamma p}^{\delta}$  for  $\delta = 0.32$ .

of the proton structure function  $F_2$  offers an indirect way to get a handle on the gluon density. This measurement was made possible by the extremely successful description of  $F_2$  by the DGLAP equations and has been presented by M. Kasemann at this conference. An alternative way is to directly tag the quark box formed in a photon-gluon collision either by identifying heavy quarks, e.g. charm via  $D^*$  or  $J/\psi$  mesons, or by measuring inclusively the 2+1 jet cross section at small  $x$ . This method has, compared to heavy flavour production, a much larger cross-section, but has the disadvantage that the background from quark initiated processes has to be subtracted statistically. Moreover, the reach to small values of  $x_{g/p} = x(1 + \hat{s}/Q^2)$  (see Fig.7 for notation) is restricted, since large invariant jets masses ( $\hat{s} > 100 \text{ GeV}^2$ ) are experimentally required to define clean jets. An extraction of the gluon density in leading order using the inclusive 2+1 jet rate achieved by the H1 collaboration<sup>33</sup> has already been presented on the last 'Physics in Collision' conference<sup>34</sup>.

Gluon initiated processes can be unambiguously pinned down by selecting events where a  $J/\psi$  is produced. The leptonic decay modes ( $J/\psi \rightarrow e^+e^-$  and  $J/\psi \rightarrow \mu^+\mu^-$ ) of this meson provide a clean experimental signature. In the elastic channels only two leptons are found in the detector, in the inelastic channel there are additional particles (see Fig. 9). Since the charm quark mass is large enough to provide a hard scale, this measurement can be performed at very low  $Q^2$  where the cross-section is large. Besides the requirement of at least

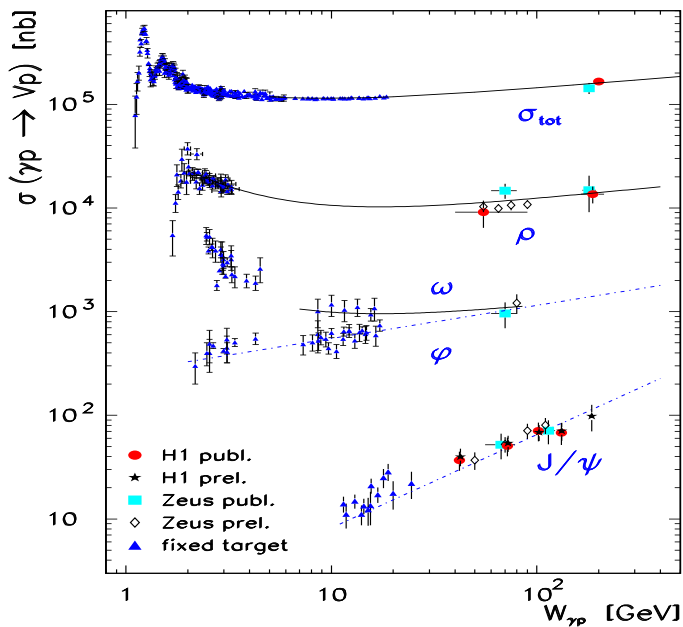


Figure 11: Total and vector meson photoproduction cross-section as function of  $W_{\gamma p}$  measured at HERA and by fixed target experiments. Superimposed is a simple parametrisation  $\sigma_{\gamma p} \sim W_{\gamma p}^{\delta}$  for  $\delta = 0.32$  (light vector mesons) and  $\delta = 0.6$  ( $J/\psi$  meson).

one additional particle in the final state, the inelastic channel can be inclusively defined using the inelasticity variable  $z = P \cdot P_{J/\psi} / (P \cdot q) < 0.8$  where  $P$  ( $q$ ) is the incoming proton (photon) momentum and  $P_{J/\psi}$  the four-momentum of the  $J/\psi$ . To avoid the phase space region where multiple emissions of gluons become more and more important and where a resummation would be required, the  $P_T^*$  of the  $J/\psi$  should exceed 2 GeV. In this region a QCD calculation<sup>35</sup> can predict the cross-section<sup>36</sup> of  $J/\psi$  production in next-to-leading order. The dependence of the cross-section on the photon-proton invariant mass ( $W_{\gamma p}$ ) and the overall normalisation is correctly described (see Fig. 10a). In this calculation the  $J/\psi$  was assumed to be produced in a colour singlet state, no room is left for an additional component of a colour octet as required by  $p\bar{p}$  data<sup>37</sup> at high energy. However, excluding the region of small  $P_T^*$ , significantly reduces the sensitivity to the small- $x$  behaviour of the gluon density as can be seen in Fig. 10a where cross-section calculations using various parametrisations are compared to data.

Previous measurements<sup>38</sup> of elastically produced  $J/\psi$  mesons revealed an exponentially falling distribution of the momentum transfer between the in-

coming and outgoing proton as expected from diffractive processes and a transverse polarisation in agreement with  $s$ -channel helicity conservation. However, the  $W_{\gamma p}$  dependence of the elastic cross-section  $\sigma_{el}$  measured over a wide range by fixed target experiments<sup>39</sup> and at HERA<sup>40</sup> exhibits a much steeper rise (see Fig. 10b) than predicted by models based on diffractive mechanisms like e.g. the one by Donnachie and Landshoff<sup>41</sup> which assumes a soft interaction in a Regge form where no quantum numbers are exchanged. This model relies on the observation that any total hadronic cross-section follows a power law with the energy available in the center of mass  $s$  like  $\sigma \sim s^\lambda$  with  $\lambda \approx 0.08$ . If one parameterizes  $\sigma_{el}$  in the region  $30 < W_{\gamma p} < 260$  GeV as  $\sigma_{el} \sim W_{\gamma p}^\delta$  one finds  $\delta = 0.6 \pm 0.12$  rather than  $\delta = 0.32$  as predicted by the Regge-inspired model. This significant rise can be better described by Ryskin's QCD inspired model<sup>42</sup> where the  $J/\psi$  couples via two gluons to the proton. To leading order it predicts that  $\sigma_{el} \sim [\alpha_s(\bar{Q}^2) \bar{x}g(\bar{x}, \bar{Q}^2)]^2$  where  $\bar{Q}^2 = 1/4M_{J/\psi}^2$  and  $\bar{x} = M_{J/\psi}^2/W_{\gamma p}^2$ . The quadratic dependence on  $g(x, Q^2)$ , makes the elastic channel of  $J/\psi$  photoproduction a sensitive discriminator for the slope of the gluon distribution  $\sigma_{el} \sim [xg(x, Q^2)]^2 \sim x^{-2\lambda} \sim W_{\gamma p}^{4\lambda}/Q^2$ . This model, including higher order corrections<sup>43</sup>, agrees with the data when using the MRSA' parametrisation<sup>44</sup> with  $\lambda = 0.17$ . The parametrisation of GRV tends to give a steeper  $W_{\gamma p}$  dependence. Since phenomenological assumptions concerning the two gluon interaction have to be made, the  $W_{\gamma p}$  dependence of  $\sigma_{el}$ , rather than the absolute normalization, is a more reliable probe of  $g(x, Q^2)$ . When comparing to HERA data, the model prediction is therefore normalized to fixed target data. A direct extraction of  $g(x, Q^2)$  seems feasible once experimental and theoretical problems are better understood.

The steep rise of  $\sigma_{el}$  with increasing  $W_{\gamma p}$  can be contrasted with the moderate increase of the total photoproduction cross-section and the cross-section of the light vector mesons  $\rho$ ,  $\omega$  and  $\varphi$  which are in excellent agreement with model predictions where only soft interactions are assumed (see Fig.11). The failure of this picture to describe elastic  $J/\psi$  production together with the success of Ryskin's model gives additional confidence in the potential of QCD to describe processes where the scales involved are still surprisingly small. The production of light and heavy vector mesons at HERA will allow to gain a better understanding of the transition from a region governed by soft interactions to a domain where perturbative QCD turns on. First indications for a similar transition when studying light vector meson production with increasing  $Q^2$  have also been observed at HERA<sup>45</sup>.

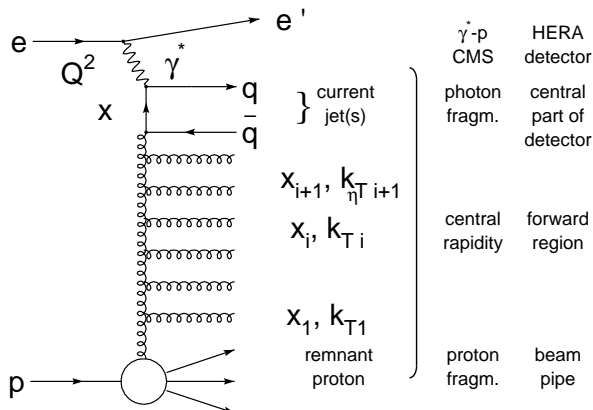


Figure 12: *Diagram of an  $e^\pm p$  collision at low  $x$ .*

### Deep-inelastic scattering at small $x$

At low  $x$  the simple picture of deep-inelastic scattering as a process where a virtual photon interacts instantaneously with a point-like parton freely moving in the proton has to be modified. Since the probability that a parton radiates becomes increasingly high at low  $x$ , the parton struck by the photon originates most likely from a cascade initiated by a parton with high longitudinal momentum. The phase space for gluon radiation is enlarged with decreasing  $x$ . Such an interaction is illustrated in Fig.12. The gluon is the driving force behind the parton cascade. The transitions  $g \rightarrow gg$  and  $g \rightarrow q\bar{q}$  at each point in the ladder can be approximated by the DGLAP equations. By resumming the LO and NLO  $(\alpha_s \ln Q^2)^n$  terms they predict the  $Q^2$  evolution of a parton known to be point-like at some given scale  $Q_0$  to the region where the interaction with the photon takes place. They describe the change in the parton density with varying spatial resolution ( $\lambda \sim 1/Q$ ) of the probe. One of the assumptions<sup>d</sup> necessary to derive the DGLAP equations is a strongly ordered configuration in the parton virtualities along the ladder connecting the soft proton constituents to the hard subprocess. This leads to a suppression of the available phase space for gluon radiation.

When the  $(\alpha_s \ln 1/x)^n$  terms become large, they have to be taken into account, e.g. by the resummation accomplished by the BFKL equations<sup>47</sup>. In a physical gauge, these terms correspond to an  $n$ -rung ladder diagram in which gluon emissions are ordered in longitudinal momentum. The strong ordering

<sup>d</sup>For a digestible introduction to low- $x$  physics see A. Martin<sup>46</sup>.

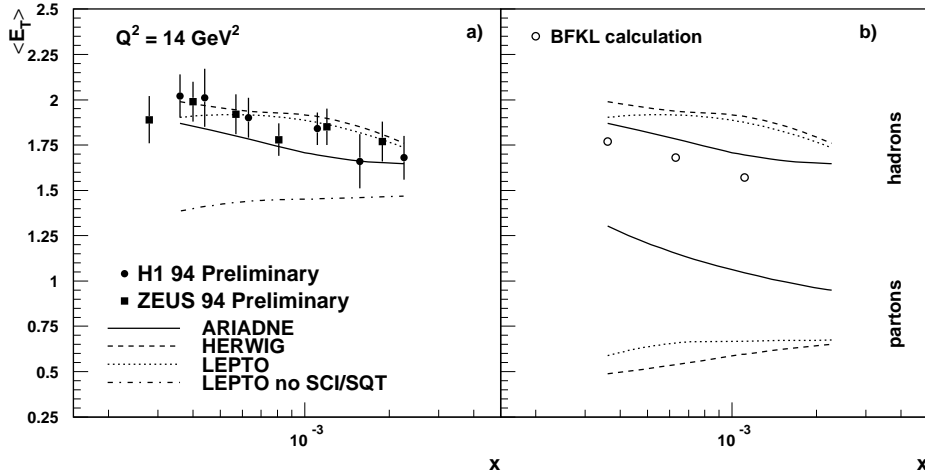


Figure 13: Mean transverse energy in  $-0.5 < \eta^* < 0.5$  measured by H1 and ZEUS (closed symbols) in the cms for  $Q^2 = 14 \text{ GeV}^2$  as function of  $x$ . Superimposed are QCD model predictions (lines) for hadrons (a) and partons (b) by QCD models and an analytic BFKL calculation (open circles) carried out on parton level only.

of the transverse momenta is replaced by a diffusion pattern as one proceeds along the gluon chain. The BFKL equations describe how a particular high momentum parton in the proton is dressed by a cloud of gluons at low  $x$  localized in a fixed transverse spatial region of the proton. At very low  $x$  it is expected that many gluons coexist and will no longer act as free partons, but interact with each other. This 'saturation' regime is characterized by an equilibrium of gluon emission and absorption. A new QCD regime is reached where individual parton-parton interactions are weak, but where the field strength becomes - due to the number of partons - so strong that perturbation theory is not reliable. It is not clear if in the HERA regime such effects could be observed.

Experimentally, it is interesting to measure observables sensitive to the underlying parton dynamics. Studying the probe after the interaction is the classical approach to get information on the structure of the target. The measurement of the proton structure function  $F_2$  has the benefit that it can be directly compared to analytical QCD calculations. The rise of  $F_2$  with decreasing  $x$  observed at HERA<sup>48</sup> appears to be well described by the DGLAP equations. Even at the lowest values of  $x$  the BFKL terms are not needed to obtain a satisfactory description.

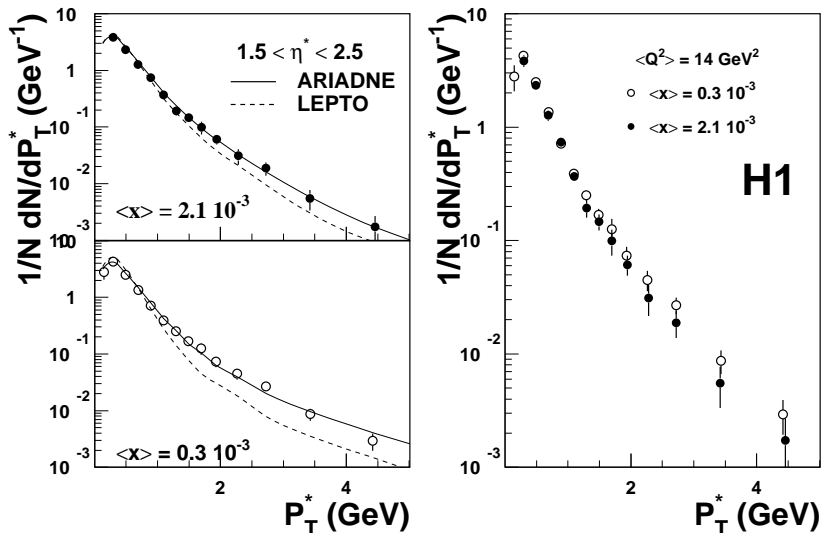


Figure 14: Transverse momentum distribution of single charged particles in  $1.5 < \eta^* < 2.5$  measured by H1 in the cms for fixed  $Q^2 = 14 \text{ GeV}^2$  and two  $x$  bins. Superimposed as lines are QCD model predictions.

However,  $F_2$  might be too inclusive to reveal the potentially small resummation effects. A better indicator might be provided by observables based on the hadronic final state emerging from the parton cascade, since they can be chosen such that the differences between the two complementary approximations are enhanced. However, predictions have then mainly to be based on Monte Carlo event generators simulating the detailed properties of the hadronic final state by including the hard subprocess, QCD radiation effects and the transition of partons to hadrons.

The LEPTO Monte Carlo<sup>49</sup> incorporates the QCD matrix element to first order in  $\alpha_s$  and approximately accounts for higher order parton emissions by the concept of parton showers<sup>52</sup> based on the DGLAP equations (MEPS model). The non-perturbative transition of the partonic final state to the observable hadrons is modeled by the LUND string mode<sup>50</sup> as incorporated in JETSET<sup>53</sup>. ARIADNE<sup>54</sup> differs only in the treatment of the hard subprocess and the QCD shower evolution. Gluon emissions are treated by the colour dipole mode<sup>55</sup> assuming a chain of independent radiating dipoles spanned by colour connected partons. The first emission in the cascade is corrected by the matrix element to first order<sup>56</sup>. A phenomenological suppression of gluons with short wavelengths (having high transverse momenta) only resolving part

of the extended colour charge distribution of the proton remnant has been introduced for DIS. This leads to a more pronounced population of partons towards the proton remnant than observed in LEPTO where the phase space is controlled by the strong ordering of the gluon virtualities and the ratio of the parton density function at each branching point. It has been argued that the partonic state as encountered in ARIADNE is more closely related to the one expected from a BFKL scenario<sup>57,58</sup>. Both Monte Carlo models are able to give a consistent picture of the event topology and provide a fair description of basic event properties<sup>59,60</sup>.

Using the hadronic final state, the presence of parton activity can be experimentally probed from the region close to the photon quark interaction down to (pseudo-)rapidities defined as  $\eta^* = -\ln \tan(\theta/2)$  where  $\theta$  is the polar angle between a particle and the proton direction<sup>e</sup>. In the cms  $\eta^* \approx -1$  can be reached beyond which the acceptance of the two main HERA detectors ends (see also Fig.12). An inclusive measure is the mean transverse energy ( $\langle E_T^* \rangle$ ) in the central region  $-0.5 < \eta^* < 0.5$ . Due to the increasing phase space with decreasing  $x$ , gluons are more abundant and  $\langle E_T^* \rangle$  is expected to rise. This behaviour is seen in the data<sup>61,62,63</sup> as is illustrated in Fig.13a where the  $\langle E_T^* \rangle$  is shown for fixed  $Q^2 = 14 \text{ GeV}^2$ . Both QCD models are able to describe the data. LEPTO, however, has to produce 60 – 80% of the  $\langle E_T^* \rangle$  during the hadronization phase to compensate for the different  $x$  dependence of the  $\langle E_T^* \rangle$  seen at the parton level as is illustrated in Fig.13. This could only be achieved by introducing two new non-perturbative production mechanisms for  $\langle E_T^* \rangle$ . In events where a sea-quark is involved in the hard subprocess, its partner is not - as in previous versions - simply rearranged to a meson or a baryon within the proton remnant, but is used to stretch a string to one of the quarks remaining untouched in the proton (SQT). The second new ingredient is the assumption of a soft colour interaction<sup>64</sup>(SCI) which changes only the colour configuration of the partonic system while leaving the colour field of the proton. This colour rotation offers, by producing a colour singlet in the final state, a possible explanation of the rapidity gap events observed at HERA and at the same time (due to longer strings caused by the colour rearrangement) the transverse energy needed to match the data. Without these two new features a constant amount of  $\langle E_T^* \rangle$  is generated during the hadronisation and the data are not described (see Fig.13). Although ARIADNE uses the same hadronisation model as LEPTO, a constant amount of only 30-40% of the  $\langle E_T^* \rangle$  is produced during hadronisation. An analytical BFKL calculation<sup>64</sup>, only carried out for partons, predicts the same  $x$  dependence as seen in the data, but lies significantly above the corresponding ARIADNE curve.

---

<sup>e</sup> The direction of the proton points along the negative  $z$ -axis in the cms.

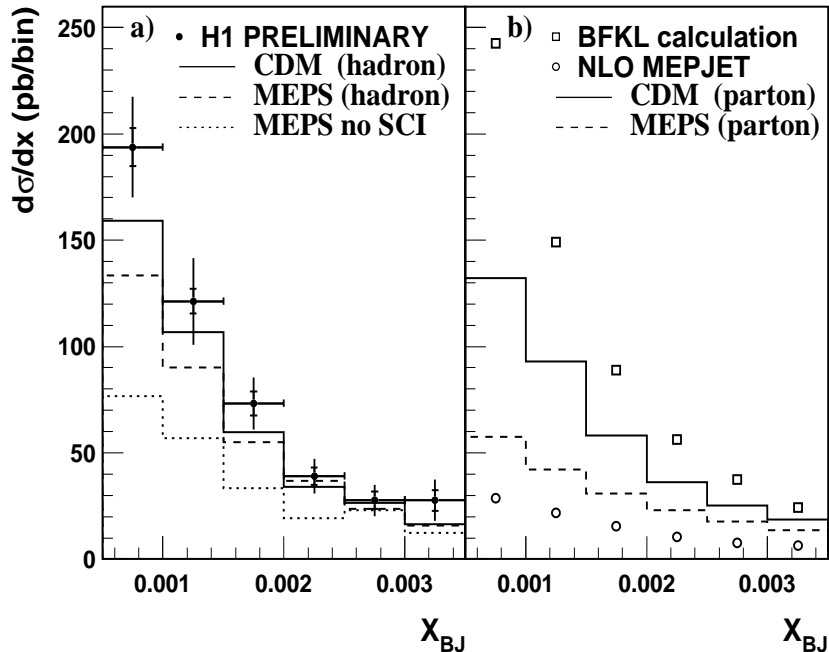


Figure 15: *Forward jet cross-section as function of  $x$  measured by H1. Superimposed are QCD model predictions for hadrons (a) and partons (b). An analytic BFKL calculation (open squares) and a NLO QCD calculation (open circles) are superimposed.*

The hard tail of the  $P_T^*$  distribution of single charged particles has been suggested<sup>65</sup> as a better tool to disentangle non-perturbative hadronisation effects from parton activity as described by perturbative QCD. This observable is more directly related to hard parton emissions and cannot be mimicked by a cumulative effect from many soft particle emissions during hadronization. The measured steeply falling  $P_T^*$  distribution in the interval  $1.5 < \eta^* < 2.5$  gets harder for decreasing  $x$  (see Fig.14). While at large  $x$  LEPTO and ARIADNE are both able to describe the data, LEPTO significantly falls below the data at low  $x$ . This indicates that more partons are produced than expected from models with suppressed parton radiation based on the DGLAP parton showers. Similar, but less conclusive, results<sup>62</sup> have been obtained by using the inclusive transverse energy distribution in  $-0.5 < \eta^* < 0.5$ .

Another signature designed to enhance BFKL effects is the production of 'forward jets',<sup>66</sup> characterized by a squared transverse momentum ( $k_T^2$ ) of the order of the photon virtuality  $Q^2$  and  $x_{jet} = E_{jet}/E_p$  as large and  $x$  as

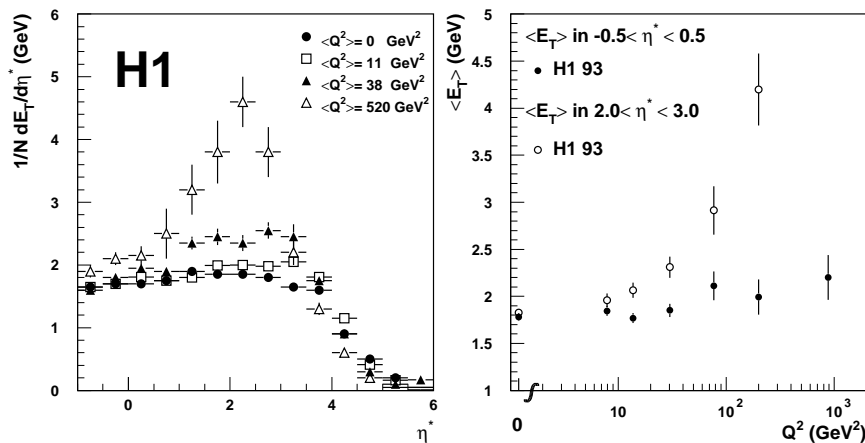


Figure 16: Energy flow at fixed  $W = 180 \text{ GeV}^2$  in the hadronic center of mass for different  $Q^2$  bins ranging from 0 to 520  $\text{GeV}^2$  and mean transverse energy for  $-0.5 < \eta^* < 0.5$  and  $2 < \eta^* < 3$  in function of  $Q^2$ .

small as kinematically possible.  $E_{\text{jet}}$  ( $E_p$ ) denotes the energy of the forward jet (proton). The first requirement suppresses the strongly ordered DGLAP evolution. Asking for large  $x_{\text{jet}}/x$ , the forward jet can be separated by a large rapidity interval from the struck quark such that the phase space of parton emission between the two is amplified. For this kinematical configuration the  $\alpha_s \ln x_{\text{jet}}/x$  terms are expected to become so large that their resummation should lead to a sizable increase of the forward jet cross-section.

A fast rise of the cross-section for forward jets defined by  $k_T > 3.5 \text{ GeV}$ ,  $0.5 < k_T^2/Q^2 < 2$  and  $x_{\text{jet}} > 0.035$  with decreasing  $x$  is seen in the H1 data<sup>68</sup> corrected to hadron level (see Fig.15a). ARIADNE falls slightly below the data, but shows the same trend towards small  $x$ . Hadronisation effects are well below 20% such that the same  $x$  dependence is also seen on parton level. While LEPTO predicts - as expected - a similar moderate increase of the forward jet cross-section as a full NLO QCD calculation<sup>67</sup> at the parton level, it is also able to describe the data by producing a large fraction of forward jets (up to 80%) in the hadronisation phase. Without assuming soft colour interaction the hadronisation corrections are similar to the ones obtained in ARIADNE, but then the data are not described (dotted line in Fig.15a). An analytical BFKL calculation<sup>69</sup> exhibits a much faster rise with  $1/x$  compared to the ARIADNE result on parton level. However, the authors point out that several effects which might lower the prediction have not been taken into account.

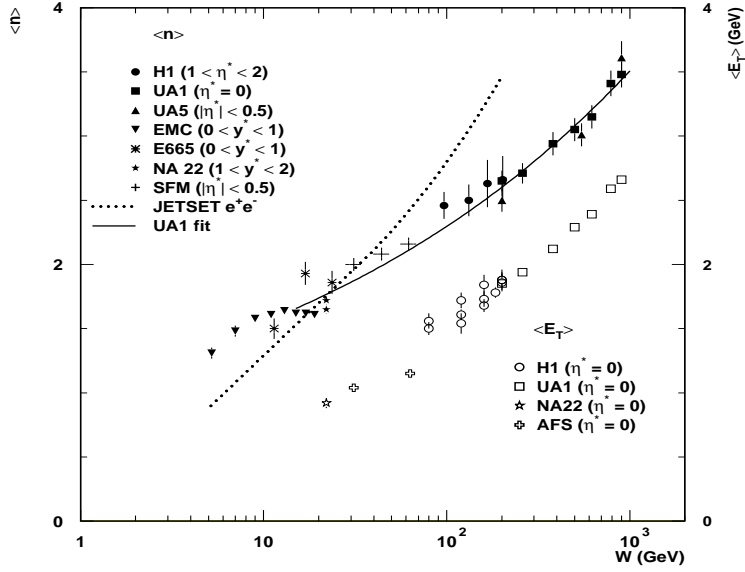


Figure 17: Mean multiplicity of charged particles in a given (pseudo-)rapidity region  $y(\eta)$  and  $\langle E_T^* \rangle$  in a central rapidity region measured in  $e^\pm p$  and  $p\bar{p}$  collisions as function of  $W$ . The solid (dotted) line indicates the behaviour of the mean charged particle multiplicity in  $p\bar{p}$  ( $e^+e^-$ ) collisions.

### Deep-inelastic scattering as hadron-hadron scattering

Strictly speaking, the physical picture of DIS as an interaction of a photon with a parton freely moving in the proton is only valid if the proton is very fast. Only in this reference frame is the interaction time of the virtual photon with the parton short compared to the interactions regularly taking place in the proton such that the photon instantaneously probes the proton content. In the reference frame where the proton is at rest and the photon is fast, it is more appropriate to imagine that the photon fluctuates into a quark anti-quark pair before interacting with the proton. If the fluctuation time is long compared to the interaction time, a parton cascade can develop and a complicated object is formed which strongly interacts with matter. Using the uncertainty principle the fluctuation time<sup>10</sup> can be calculated to  $\tau_\gamma = 1/(m_p x)$  where  $m_p$  is the proton mass. For a typical  $x$  value of  $10^{-3}$ , the distance before the photon interacts with the target is  $c\tau_\gamma \approx 200$  fm which is large compared to the proton radius of about 1 fm.

If one chooses suitable observables, one can therefore find in DIS at low- $x$  characteristic properties of hadron-hadron collisions. Changing the photon virtuality from  $\approx 0$  to about  $520 \text{ GeV}^2$ , the transverse energy flow<sup>70</sup> in the hadronic cms for fixed  $W = 180 \text{ GeV}$  varies only in the region where the hard subprocess has taken place (see Fig.16a). The  $\langle E_T^* \rangle$  in  $2 < \eta^* < 3$  indeed

grows with  $Q^2$  as is depicted in Fig.16b. Surprisingly, this rise only starts at about  $10 \text{ GeV}^2$ . The measured  $\langle E_T^* \rangle$  produced in collisions with on-shell photons, which cannot be treated perturbatively, has the same magnitude as observed in a high  $Q^2$  region where first calculations have been very promising. In the central rapidity region of  $-0.5 < \eta^* < 0.5$  however,  $\langle E_T^* \rangle$  is only little influenced by the virtuality of the photon. The impact of the photon virtuality penetrates only  $\Delta\eta^* \approx 1.5$ . This is typical of the short range correlation in inelastic hadron-hadron collisions. When comparing the  $\langle E_T^* \rangle$  to hadron-hadron collisions, it scales with the center of mass energy of the collision independent of the nature of the incoming particles. This is shown in Fig.17. It is interesting to note that also the mean charged particle multiplicity exhibits a similar dependence on  $W$ . Also here the DIS data from HERA<sup>71</sup> interpolate - despite the slightly different rapidity regions - between previous fixed target data and hadron-hadron collisions at much higher energy (see Fig.17). This suggests a universal behaviour of the dynamics in the central rapidity region. In  $e^+e^-$  collisions a steeper dependence on  $W$  is seen for these rapidity regions (dotted line in Fig.17).

Since DIS data reveal some properties of soft hadron-hadron interactions there is some hope that the understanding of DIS at low  $x$  by perturbative QCD can give a handle on the understanding of the underlying dynamics of strong interactions. If the first attempts to understand in perturbative QCD some low- $x$  HERA data are successful, a tool might become available to provide a universal description of strongly interacting particles from an perturbative theory of asymptotically free partons at short distances to the theory of the confined hadrons at long distances.

### Acknowledgments

It is a pleasure to thank my colleagues from the H1 and ZEUS collaboration for providing me with the latest data and information. I have profited from many stimulating discussions with M. Kuhlen and E. DeWolf and I gratefully appreciate their careful reading of the manuscript. I deeply acknowledge the support of the physics coordinators of the H1 and ZEUS collaboration, J. Dainton and R. Nania, and would like to thank them for their helpful comments.

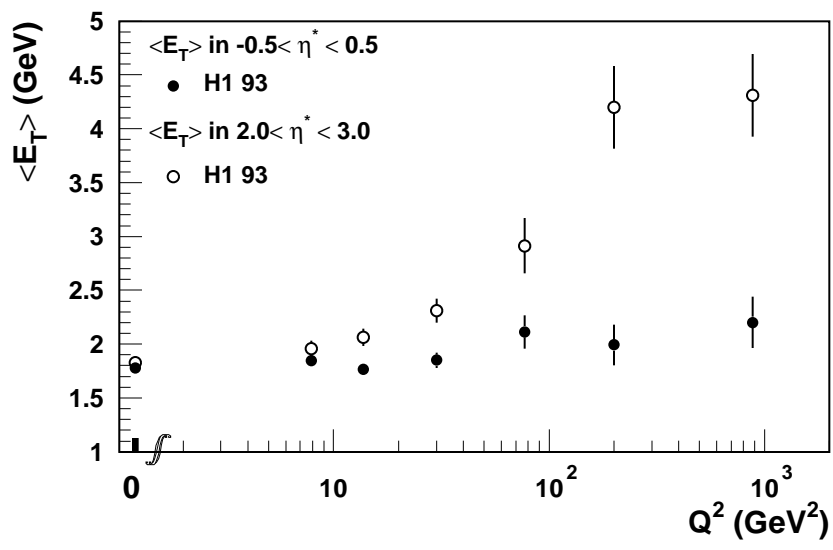
### References

1. H1 Collab., S. Aid et al., Phys. Lett. B353 (1995) 578; ZEUS Collab., Prelim. results, see M. Kasemann in these proceedings.
2. H1 Collab., I. Abt et al., Z. Phys C 63 (1994) 377.
3. ZEUS Collab., M.Derrick et al. Z. Phys. C70 (1996) 1.

4. EMC Collab., A. Arnedodo et al., Z. Phys. C36 (1987) 527.
5. N. Magnussen et al., Proc. of the HERA workshop 1991, ed. G. Ingelmann and W. Buchmüller, Vol. 3, Hamburg 1992, p. 1167.
6. H1 Collab., S. Aid et al., Nucl. Phys. B445 (1995) 3.
7. ZEUS Collab., M.Derrick et al. Z. Phys. C67 (1995) 93.
8. MARK1 Collab., J.L. Siegrist et al., Phys. Rev. D26 (1986) 969; OPAL Collab., P.D. Acton et al., Z. Phys C53 (1992) 539; PLUTO Collab., C. Berger et al., Phys. Lett. B95 (1980) 313; TASSO Collab., W. Braunschweig et al., Z. Phys. C45 (1989) 193.
9. FNAL Collab., M. Derrick et al., Phys. Lett. B91 (1980) 470.
10. Y. L. Dokshitzer et al., *Basics of perturbative QCD*, Editions Frontieres, Gif-sur-Yvette, 1991.
11. TASSO Collab., W. Braunschweig et al., Z. Phys. C67 (1995) 81; Z. Phys. C22 (1984) 307; OPAL Collab., M. Akraway et al., Phys.Lett. B247 (1990) 617; TOPAZ Collab., R. Itoh et al., Phys. Lett. B345 (1995) 335.
12. H1 Collab., S. Aid et al., Nucl. Phys. B445 (1995) 3.
13. R.D. Ball and S. Forte, Phys.Lett. B358 (1995) 365.
14. DELPHI Collab., P. Aarnio et al., Phys. Lett. B311 (1993) 408.
15. ZEUS Collab., M. Derrick et al., Z. Phys. C67 (1995) 93.
16. N. Brook, Proc. of the Int. Workshop on DIS and Related Phenomena, ed. G. D'Agostini and A. Nigro, Rome, 1996 and ZEUS Collab., PA02-034 contr. to ICHEP'96, Warsaw, Poland, July 1996.
17. D. Graudenz, Proc. of 'Future Physics at HERA', ed. G. Ingelmann, A. De Roeck and R. Klanner, Hamburg 1996, p. 533.
18. D. Graudenz, Phys. Lett. B256 (1991) 518; Phys. Rev. D49 (1994) 3291; T. Brodtkorb and J. G. Körner, Z. Phys. C54 (1992) 141.
19. JADE Collab., W. Bartel et al., Z. Phys. C33 (1986) 23.
20. H1 Collab., T. Ahmed et al., Phys. Lett. B346 (1995) 415.
21. ZEUS Collab., M. Derrick et al., Phys. Lett. B363 (1995) 201.
22. Particle Data Group, R.M. Barnett et al., Phys. Rev. D54 (1996).
23. J. Chyla and J. Rames, Proc. of 'Future Physics at HERA', ed. G. Ingelmann, A. De Roeck and R. Klanner, Hamburg 1996, 529.
24. E. Mirkes and D. Zeppenfeld, Phys. Lett. B380 (1996) 205.
25. J. Huth et al., in Proc. Summer Study on HEP, Snowmass, 1990.
26. S. Catani, Y. Dokshitzer and B. Webber, Phys. Lett. B285 (1992) 291.
27. E. Mirkes and D. Zeppenfeld, TTP 96-10, MADPH-96-935, invited talk given at the Cracow Epiphany Conference on Proton Structure, Jan 1996.
28. T. Trefzger, Proc. of the Int. Workshop on DIS and Related Phenomena, ed. G. D'Agostini and A. Nigro, Rome, 1996.

29. Yu. L. Dokshitzer, Sov. Phys. JETP 46 (1977) 641; V.N. Gribov and L.N. Lipatov, Sov. J. Nucl. Phys. 15 (1972) 438 and 675; G. Altarelli and G. Parisi, Nucl. Phys. 126 (1977) 297.
30. A.D. Martin, R.G. Roberts and W.J. Stirling, Phys. Rev. D 50 (1994) 6734 and Phys. Lett. B354 (1995) 155.
31. CTEQ Collab., H.L. Lai et al., Phys. Rev. D51 (1995) 4763.
32. M. Glück, E. Reya and A. Vogt, Z. Phys. C67 (1995) 433.
33. H1 Collab., S. Aid et al., Nucl. Phys. B449 (1995) 3.
34. U. Görlach, DESY 95-207, Hamburg 1995.
35. M. Krämer et al., Phys. Lett. B348 (1995) 657; M. Krämer, Nucl. Phys. B459 (199) 3.
36. H1 Collab., S. Aid et al., PA02-085 contr. to ICHEP'96, Warsaw, July 1996; ZEUS Collab., M. Derrick et al., Phys. Lett. B350 (1995) 120 and PA02-047 contr. to ICHEP'96, Warsaw, July 1996;
37. M. Cacciari and M. Krämer, Phys. Rev. Lett.76 (1996) 4128.
38. H1 Collab., S. Aid et al., Nucl.Phys. B472 (1996) 3.
39. E687 Collab., P.L. Frabetti et al., Phys. Lett. B316 (1993) 197; E401 Collab., M. Binkley et al., Phys. Rev. Lett. 48 (1982) 73; FTPS Collab., B. H. Denby et al., Phys. Rev. Lett. 52 (1884) 795.
40. H1 Collab., S. Aid et al., PA02-085 contr. to ICHEP'96, Warsaw, July 1996. ZEUS Collab., M. Derrick et al., Phys. Lett. B350 (1995) 120 and PA02-047 contr. to ICHEP'96, Warsaw, July 1996.
41. A. Donnachie and P.V. Landshoff, Phys. Lett. B348 (1995) 213; *ibid.* B296 (1992) 227.
42. M.G. Ryskin, Z. Phys. C57 (1993) 89.
43. M.G. Ryskin et al., DTP/95/96 and hep-ph/9511228.
44. A.D. Martin, W.J. Stirling and R.G. Roberts Phys.Rev.D51 (1995) 4756. DTP/95/96 and hep-ph/9511228.
45. ZEUS Collab., M. Derrick et al., Phys. Lett. B356 (1995) 601.
46. A. Martin, Lectures given at the XXI Int. Meeting on Fundamental Physics, Miraflores de la Sierra, Madrid, 1993 and DTP/93/66, August 1993.
47. E.A. Kuraev, L.N. Lipatov and V.S. Fadin, Sov. Phys. JETP 45 (1972) 199; Y.Y. Balitsky and L.N. Lipatov, Sov. J. Nucl. Phys. 28 (1978) 282.
48. H1 Collab., S. Aid et al., Nucl. Phys. B470 (1996) 3; ZEUS Collab., M. Derrick et al., Z. Phys. C69 (1996) 607.
49. G. Ingelman, in Proc. HERA workshop, Eds. W. Büchmüller and G. Ingelman, Hamburg (1991) Vol. 3, 1366; G. Ingelman, A. Edin and J. Rathsmann, DESY-96057, Hamburg, April 1996.
50. B. Andersson et al., Phys. Rep. 97 (1983) 31.

51. A. Edin, G. Ingelman and J. Rathsmann, DESY 96-060, Hamburg, April 1996.
52. M. Bengtsson and T. Sjöstrand, Z. Phys. C37 (1998) 465; M. Bengtsson, G. Ingelman and T. Sjöstrand, Proc. of the HERA workshop 1987, ed. R.D. Peccei, DESY, Hamburg Vol. 1 (1988) 149.
53. T. Sjöstrand, Computer Phys. Comm. 39 (1986) 347; T. Sjöstrand and M. Bengtsson, *ibid.* 43 (1987) 367; T. Sjöstrand, CERN-TH-6488 (1992) and CERN-TH 7112 Dec. 1993.
54. L. Lönnblad, Computer Phys. Comm. 71 (1992) 15.
55. G. Gustafson and U. Peterson, Nucl. Phys. B306 (1988); G. Gustafson, L. Lönnblad and U. Peterson, Z. Phys. C43 (1989) 625.
56. L. Lönnblad, Z. Phys. C65 (1995) 285.
57. A. H. Mueller, Nucl. Phys. B 415 (1994) 373.
58. J. Rathsmann, SLAC-PUB-7344, October 1996.
59. T. Carli, Proc. of the Int. Workshop on DIS and Related Phenomena, ed. G. D'Agostini and A. Nigro, Rome, 1996.
60. N. Brook et al., Proc. of 'Future Physics at HERA', ed. G. Ingelmann, A. De Roeck and R. Klanner, Hamburg 1996, 613.
61. H1 Collab., S. Aid et al., Phys. Lett. B356 (1995) 118.
62. H1 Collab. contrib. PA02-073 to the 28th ICHEP'96, Warsaw, July 1996.
63. N. Pavel, Proc. of the Int. Workshop on DIS and Related Phenomena, ed. G. D'Agostini and A. Nigro, Rome, 1996.
64. K. Golec-Biernat, J. Kwieciński, A.D. Martin and P. Sutton, Phys. Lett. B335 (1994) 220, and P. Sutton private communication.
65. M. Kuhlen, Phys. Lett. B382 (1996) 441.
66. A.H. Mueller, Nucl. Phys. B (Proc. Suppl.) 18C (1990) 125; J. Pys. G17 (1991) 1443 and J. Bartels, A. de Roeck and M. Loewe, Z. Phys. C54 (1992) 635.
67. E. Mirkes, private communication.
68. H1 Collab., S. Aid et al., PA03-049 contr. to ICHEP'96, Warsaw, July 1996.
69. J. Bartels et al., Phys. Lett. B384 (1996) 300.
70. H1 Collab., S. Aid et al., Phys. Lett. B358 (1995) 412.
71. H1 Collab., S. Aid et al., DESY-96-215, Hamburg, 1996.



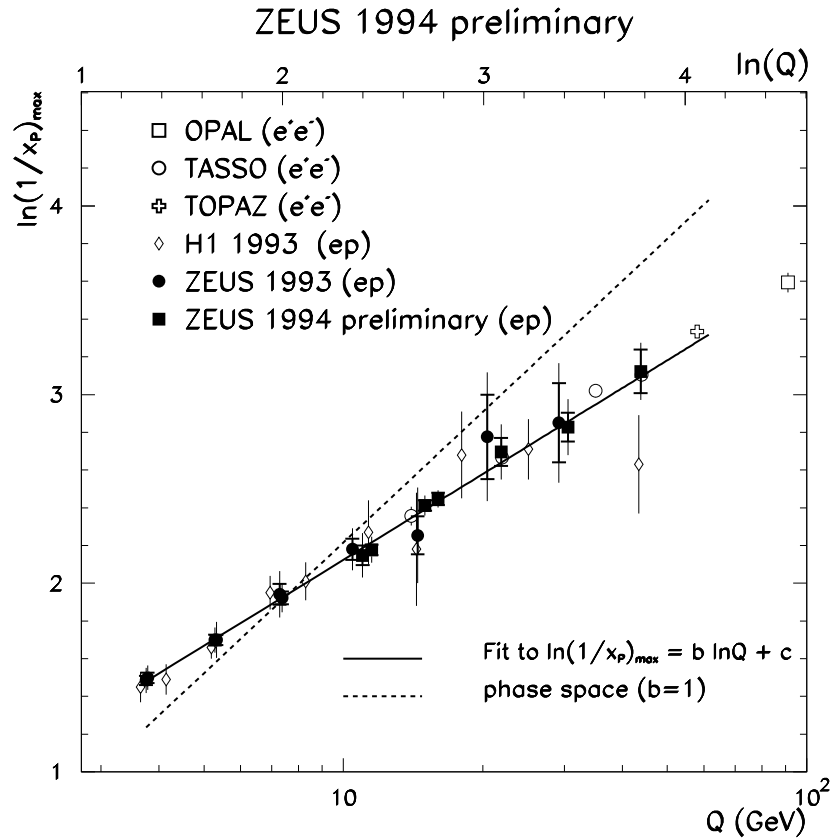


Figure 2:  $\ln(1/x_p)_{max}$  as a function of  $Q$ . The ZEUS (1993 & 1994) and H1 data are compared to results from OPAL, TASSO and TOPAZ. A straight line fit of the form  $\ln(1/x_p)_{max} = b \ln(Q) + c$  to the ZEUS  $\ln(1/x_p)_{max}$  values is indicated as well as the line corresponding to  $b = 1$ , discussed in the text.

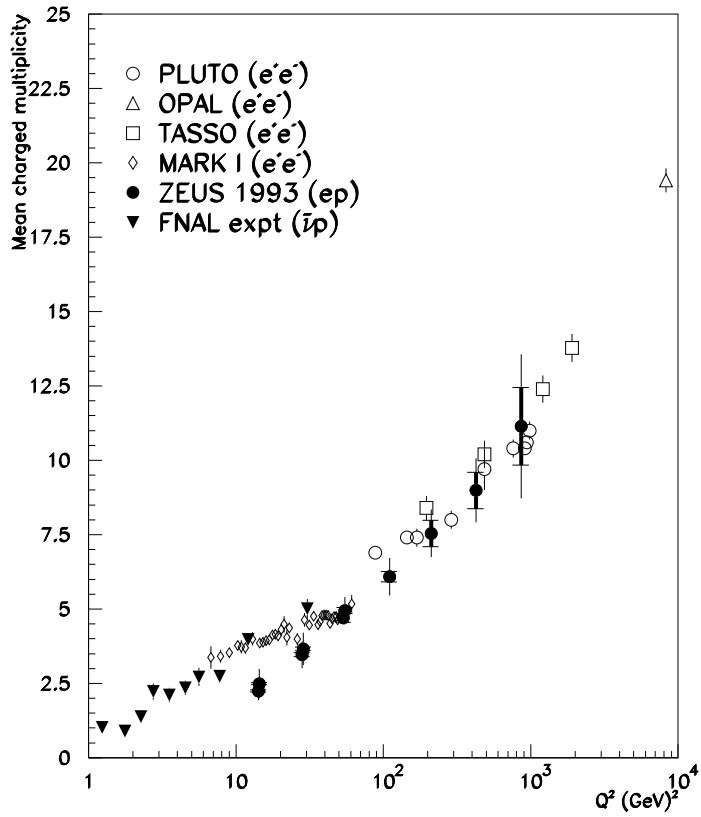


Figure 1: Twice the measured charged particle multiplicity (for  $x \sim 10^{-3}$ ) in the current region of the Breit frame as measured in DIS by this experiment and by the FNAL  $\bar{\nu}p$  experiment at  $x \sim 0.1$ . The factor of two arises from the fact that there is a  $q\bar{q}$  pair in  $e^+e^-$  compared to a single quark in DIS. Also shown are the results from  $e^+e^-$  experiments.

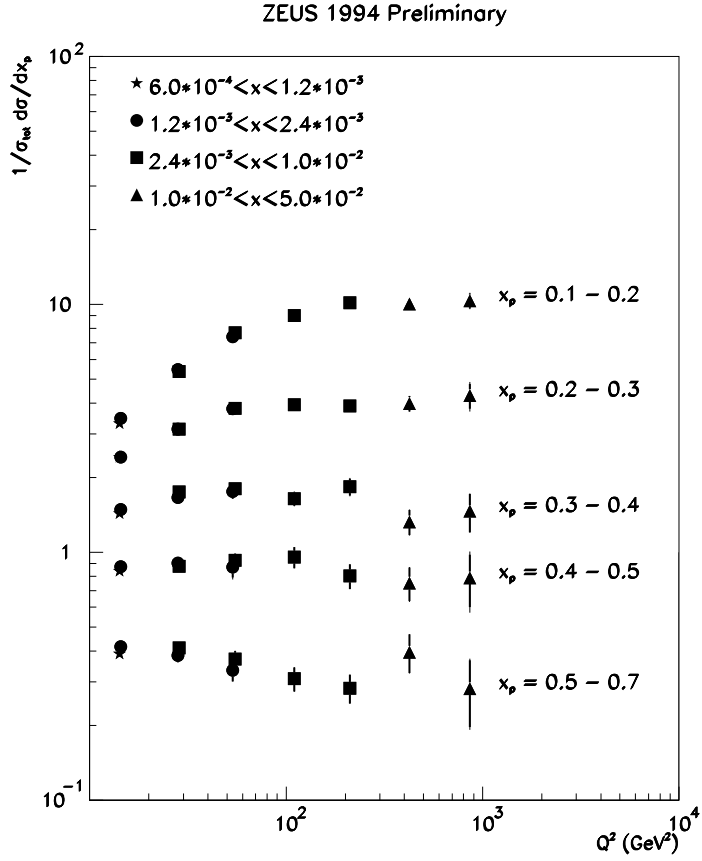


Figure 3: Preliminary inclusive scaled momentum cross section in the Breit current region for  $ep \rightarrow eX$  from this experiment. The different symbols represent the different  $x$ -bins.